AN EXPERIMENTAL VALIDATION OF THE NEAR-FIELD - FAR-FIELD TRANSFORMATION WITH SPHERICAL SPIRAL SCAN

F. D'Agostino (1), F. Ferrara (1), J.A. Fordham (2), C. Gennarelli (1), R. Guerriero (1), M. Migliozzi (1)

(1) D.I.E.I.I. - University of Salerno, via Ponte Don Melillo, 84084 Fisciano (SA), Italy
(2) MI Technologies, 1125 Satellite Blvd, Suite 100 Suwanee, Georgia 30024-4629, USA

ABSTRACT

This work concerns the experimental validation of a probe compensated near-field – far-field transformation technique using a spherical spiral scanning, which allows one to significantly reduce the measurement time by means of continuous and synchronized movements of the positioning systems of the probe and antenna under test. Such a technique relies on the nonredundant sampling representations of the electromagnetic fields and makes use of a two-dimensional optimal sampling interpolation formula to recover the near-field data needed to perform the classical spherical near-field – far-field transformation. The good agreement between the so reconstructed far-field patterns and those obtained via the classical spherical near-field – far-field transformation assesses the effectiveness of the approach.

Keywords: Antenna measurements, Near-field – far-field transformation techniques, Spherical spiral scanning, Nonredundant sampling representations of electromagnetic fields.

1. Introduction

As well-known, near-field – far-field (NF–FF) transformation techniques play a significant role in modern antenna measurements [1-6]. In fact, they allow the overcoming of all those drawbacks which make unpractical the radiation pattern measurement of electrically large antennas in a conventional FF range. Among the NF–FF transformations, that employing the spherical scanning has attracted a considerable interest [7-14], since it gives the full antenna pattern coverage, although the data processing is remarkably burdensome than that required in the planar and cylindrical scanning cases. For what concerns the data acquisition, continuous and synchronized movements of the positioning systems of the probe and antenna under test (AUT) make the measurement set-up simpler and allow the reduction of the time required for the scanning [15]. Accordingly, NF–FF transformations using innovative spherical spiral scannings have been recently developed [16-19]. They are based on the nonredundant sampling representations of electromagnetic (EM) fields [20] and use appropriate optimal sampling interpolation (OSI) formulas [21] to reconstruct the NF data needed by the NF–FF transformation with spherical scanning [10] from the nonredundant samples acquired on the spiral. In particular, the nonredundant sampling representation on the sphere from samples collected along the spiral and the related OSI expansion have been developed in [16, 17] by assuming the AUT enclosed in the smallest sphere able to contain it and choosing the spiral step equal to the corresponding sample spacing required to interpolate the data along a meridian. Then, NF–FF transformations with spherical spiral scanning tailored for electrically long or quasi-planar antennas have been proposed in [18, 19] by properly applying the unified theory of spiral scanning for nonspherical antennas [22]. They use effective source modellings particularly suitable when dealing with AUTs having two of their dimensions very different from the third one, but which remain quite general since contain the spherical modelling as particular case. In particular, a prolate and an oblate ellipsoid has been adopted in [18] for modelling an elongated and a quasi-planar antenna, respectively. Whereas in [19], an AUT with a predominant dimension has been considered as enclosed in a "rounded cylinder" (a cylinder ended in two half spheres) and a "double bowl" (a surface formed by two circular bowls with same aperture diameter but different lateral bends) has been used to model an AUT having two predominant dimensions.

The aim of this work is to experimentally validate the NF–FF transformation technique with spherical spiral scanning based on the spherical AUT modelling. Such a validation has been carried out at the Antenna Characterization Lab of University of Salerno, equipped with a roll over azimuth spherical NF facility system supplied by MI Technologies. The comparison between the FF patterns reconstructed from the data directly measured on the classical spherical grid and those recovered from nonredundant measurements acquired on the spherical spiral has shown that the spherical spiral scanning allows one to reduce the time required for the data acquisition retaining the accuracy of the classical approach.

2. Nonredundant representation over a sphere from samples acquired on a spiral

Let us consider an AUT and a nondirective probe scanning a spiral wrapping a sphere of radius d in the antenna NF region and adopt the spherical coordinate system (r,ϑ,φ) for denoting an observation point P (Fig. 1). Since the voltage V measured by such a kind of probe has the same effective spatial bandwidth as the field [23], the theoretical results on the nonredundant sampling representation of EM fields [20] can be applied to it. Accordingly, by modelling the AUT as enclosed in the smallest sphere Σ of radius a able to contain it and by describing the spiral by means of a proper analytical parameterization $\underline{r}=\underline{r}(\eta)$, the probe "reduced voltage"

$$\tilde{V}(\eta)=V(\eta)\,\mathrm{e}^{\mathrm{j}\psi(\eta)}, \tag{1}$$

where $V(\eta)$ is the voltage V_1 or V_2 measured by the probe or by the rotated probe and $\psi(\eta)$ is a phase function to be determined, can be closely approximated by a spatially bandlimited function. The corresponding bandlimitation error becomes negligible as the bandwidth exceeds a critical value W_η [20], so that it can be effectively controlled by choosing a bandwidth equal to $\chi' W_\eta$, where χ' is an excess bandwidth factor, slightly greater than unity for electrically large antennas.

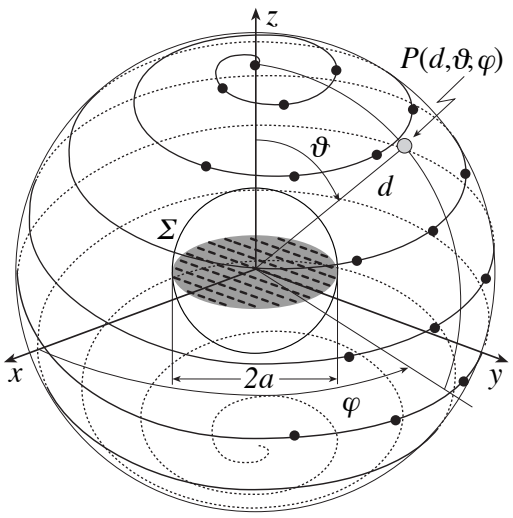

Figure 1 – Spherical spiral scanning.

The theoretical results in [17] allow the development of the voltage representation on the sphere from a nonredundant number of its samples collected along the spiral. To this end, it is necessary: i) to choose the angular elevation step of the spiral coincident with the sample spacing needed for the interpolation along a meridian; ii) to determine a nonredundant representation along the spiral, based on the theoretical results in [20].

According to [20], the sample spacing $\Delta\vartheta$ needed to interpolate the voltage along a meridian when adopting a spherical AUT modelling is

$$\Delta\vartheta=2\pi/(2M''+1) \tag{2}$$

where $M''=\mathrm{Int}(\chi M')+1$, $M'=\mathrm{Int}(\chi'\beta a)+1$, $\mathrm{Int}(x)$ denotes the integer part of x, β is the wavenumber, and $\chi>1$ is an oversampling factor [21], which allows the control of the truncation error. Therefore, the equations of the spiral are:

$$\begin{cases} x=d\sin\theta\cos\phi \\ y=d\sin\theta\sin\phi \\ z=d\cos\theta \end{cases} \tag{3}$$

where ϕ is the parameter describing it and $\theta=k\phi=\phi/(2M''+1)$. Note that the spiral angle θ, unlike the zenithal angle ϑ, can assume negative values. In fact, when the spiral describes a complete round on the surface, θ varies in the range $[-\pi,\pi]$. Moreover, the spiral angle ϕ is always continuous, whereas, according to (3), the azimuthal angle φ exhibits a discontinuity jump of π when the spiral crosses the poles. Such a curve can be obtained by radially projecting on the surface the corresponding spiral wrapping the sphere modelling the AUT.

A nonredundant sampling representation of the voltage on the spiral can be obtained by using the following expressions for the optimal phase function and parameterization [20]:

$$\psi=\psi(\eta)=\frac{\beta}{2}\int_0^s\left[\max_{\underline{r}'}\hat{R}\cdot\hat{t}+\min_{\underline{r}'}\hat{R}\cdot\hat{t}\right]\mathrm{d}s \tag{4}$$

$$\eta=\frac{\beta}{2W_\eta}\int_0^s\left[\max_{\underline{r}'}\hat{R}\cdot\hat{t}-\min_{\underline{r}'}\hat{R}\cdot\hat{t}\right]\mathrm{d}s \tag{5}$$

where $\underline{r}'$ denotes the source point, s is the arclength of the spiral, $\hat{t}$ is the unit vector tangent to it at the generic point Q, and $\hat{R}$ is the unit vector pointing from the source point to Q.

The extreme values of $\hat{R}\cdot\hat{t}$ in (4) and (5) are determined by considering the intersection of the plane defined by $\hat{t}$ and the unit vector $\hat{r}$ with the cone having the vertex at Q and the generatrices coincident with the tangents to the sphere modelling the AUT. Denoting by $\hat{R}_{1,2}$ the related unit vectors and by ε the angle between $\hat{r}$ and $\hat{t}$ (Fig. 2), we get [17]:

$$(\hat{R}_1+\hat{R}_2)/2=\hat{r}\sin\delta=\hat{r}\sqrt{1-a^2/r^2} \tag{6}$$

$$(\hat{R}_1-\hat{R}_2)\cdot\hat{t}/2=\cos\delta\sin\varepsilon=(a/r)\sin\varepsilon \tag{7}$$

By substituting (6) in (4), and taking into account that

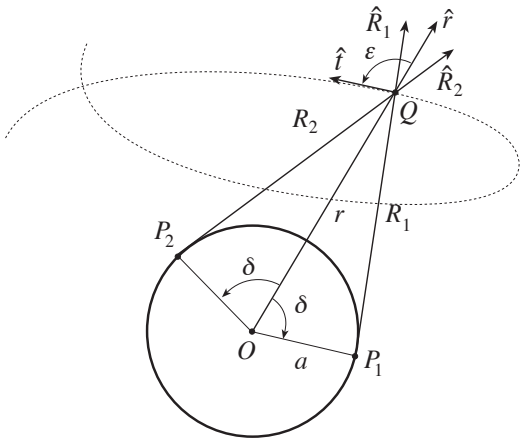

Figure 2 – Geometry in the plane $\hat{t}$, $\hat{r}$.

$\mathrm{d}r = \hat{r}\cdot\hat{t}\,\mathrm{d}s$, it results:

$$\psi = \beta\int_0^r \sqrt{1-a^2/r^2}\,\mathrm{d}r = \beta\sqrt{r^2-a^2} - \beta a\cos^{-1}\left(\frac{a}{r}\right) \quad (8)$$

On the other hand [17],

$$\mathrm{d}s = \sqrt{r^2\sin^2\theta + k^2r^2 + k^2\dot{r}^2}\,\mathrm{d}\phi \quad (9)$$

$$\sin\varepsilon = \sqrt{1-(\hat{r}\cdot\hat{t})^2} \quad (10)$$

wherein $\dot{r} = \mathrm{d}r/\mathrm{d}\theta$ and

$$\hat{r}\cdot\hat{t} = \frac{\mathrm{d}r}{\mathrm{d}s} = \frac{\mathrm{d}r}{\mathrm{d}\phi}\frac{\mathrm{d}\phi}{\mathrm{d}s} = \left[\frac{\mathrm{d}r}{\mathrm{d}\theta}\frac{\mathrm{d}\theta}{\mathrm{d}\phi}\right]\frac{\mathrm{d}\phi}{\mathrm{d}s} = k\dot{r}\frac{\mathrm{d}\phi}{\mathrm{d}s} = \frac{k\dot{r}}{\sqrt{r^2\sin^2\theta + k^2r^2 + k^2\dot{r}^2}} \quad (11)$$

By taking into account (10) and substituting (7) and (9) in (5), it results:

$$\eta = \frac{\beta a}{W_\eta}\int_0^\phi \sqrt{k^2+\sin^2 k\phi}\,\mathrm{d}\phi \quad (12)$$

It is worthy to note that the expression (8) of the phase function ψ relevant to the sampling representation along the spiral coincides with that relevant to the representation along a meridian curve [20]. Moreover, since in the considered case the spiral wraps a spherical surface, the phase function is constant and there is no need to extract the phase factor $\mathrm{e}^{-\mathrm{j}\psi}$ from the voltage expression.

According to (12), η is β/W_η times the arclength along the spiral which wraps the sphere modelling the AUT. Since such a spiral is a closed curve, it is convenient to choose the bandwidth W_η such that η covers a 2π range when the whole projecting curve on the sphere is described. As a consequence,

$$W_\eta = \frac{\beta a}{\pi}\int_0^{(2M''+1)\pi} \sqrt{k^2+\sin^2 k\phi}\,\mathrm{d}\phi \quad (13)$$

By taking into account the above representation, the OSI formula for reconstructing the reduced voltage at any point Q of the spiral is [16, 17]:

$$\tilde{V}(\eta) = \sum_{n=n_0-p+1}^{n_0+p} \tilde{V}(\eta_n)\,\Omega_N(\eta-\eta_n)\,D_{N''}(\eta-\eta_n) \quad (14)$$

where $n_0 = \mathrm{Int}(\eta/\Delta\eta)$ is the index of the sample nearest (on the left) to the point Q, $2p$ the number of retained samples $\tilde{V}(\eta_n)$, and

$$\eta_n = n\,\Delta\eta = 2\pi n/(2N''+1) \quad (15)$$

with $N'' = \mathrm{Int}(\chi N')+1$ and $N' = \mathrm{Int}(\chi' W_\eta)+1$. Moreover,

$$D_{N''}(\eta) = \frac{\sin\left[(2N''+1)\eta/2\right]}{(2N''+1)\sin(\eta/2)} \quad (16)$$

and

$$\Omega_N(\xi) = \frac{T_N\left[2\cos^2(\eta/2)/\cos^2(\bar{\eta}/2)-1\right]}{T_N\left[2/\cos^2(\bar{\eta}/2)-1\right]} \quad (17)$$

are the Dirichlet and Tschebyscheff sampling functions, $T_N(\cdot)$ being the Tschebyscheff polynomial of degree $N = N''-N'$ and $\bar{\eta} = p\,\Delta\eta$. It must be stressed that, when interpolating the voltage in the neighbourhood of the poles ($\vartheta = 0$ and $\vartheta = \pi$), the enlargement bandwidth factor χ' must be properly increased to avoid a significant growth of the band-limitation error. This is due to the fact that small variations of η correspond to very large changes of ϕ in these zones.

The OSI formula (14) can be applied to evaluate the reduced voltage values at the intersection points between the spiral and the meridian passing through the observation point P. Once these intermediate samples have been determined, the reduced voltage at P can be reconstructed via the following OSI formula:

$$\tilde{V}(\vartheta,\varphi) = \sum_{m=m_0-q+1}^{m_0+q} \tilde{V}(\vartheta_m)\,\Omega_M(\vartheta-\vartheta_m)\,D_{M''}(\vartheta-\vartheta_m) \quad (18)$$

wherein $m_0 = \mathrm{Int}\left[(\vartheta-\vartheta_0)/\Delta\vartheta\right]$ is the index of sample nearest (on the left) to P, $2q$ is the number of retained intermediate samples $\tilde{V}(\vartheta_m)$, and

$$\vartheta_m = \vartheta_m(\varphi) = k\varphi + m\,\Delta\vartheta = \vartheta_0 + m\Delta\vartheta \quad (19)$$

It is so possible to recover the data needed to perform the NF–FF transformation with spherical scanning.

3. Experimental validation

Some experimental tests assessing the validity of the described NF–FF transformation with spherical spiral scanning are reported in this section. They have been carried out in the anechoic chamber of the Antenna Characterization Lab of the University of Salerno, which is provided with a roll over azimuth spherical NF facility supplied by MI Technologies. The chamber, whose dimensions are $8\text{m}\times5\text{m}\times4\text{m}$, is covered with pyramidal absorbers ensuring a background noise lower than – 40 dB. The amplitude and phase measurements are carried out by means of a vectorial network analyzer. An open-ended WR90 rectangular waveguide is used as probe. The antenna employed in the experimental tests is a MI-12-8.2 standard gain horn with aperture $19.4\,\text{cm}\times14.4\,\text{cm}$, located on the plane $z = 0$ of the adopted reference system (Fig. 1) and operating at 10 GHz. Such an AUT has been modelled as enclosed in a sphere having radius a = 12.3 cm and the probe output voltages have been collected on a sphere of radius d = 78.5 cm.

The amplitudes of the reconstructed voltages V_1 and V_2 relevant to the meridians at $\varphi = 0°$ and $\varphi = 90°$, respectively, are compared in Figs. 3 and 4 with those directly measured on the same meridians, to assess the effectiveness of the two-dimensional OSI algorithm. For completeness, the comparison between the phase of the reconstructed voltage V_2 and that directly measured on the meridian at $\varphi = 90°$ is also reported in Fig. 5. As can be seen, there is a very good agreement between the reconstructed voltages (crosses) and the measured ones (solid line), save for the peripheral zone (below about –50 dB), wherein the error is caused by the environmental reflections.

It is worth noting that it has been necessary to increase χ' when interpolating nearby the poles in order to reduce the interpolation error. In particular, we have adopted, in the zones of the spiral determined by the 24 samples around the poles, an excess bandwidth factor such that the sample spacing is reduced by a factor 7.

At last, the FF patterns in the principal planes E and H reconstructed from the NF data acquired by using the spiral scanning are compared in Figs. 6 and 7 with those (references) obtained from the NF data directly measured on the classical spherical grid. In both the cases, the software package MI-3000 has been used to get the FF reconstructions. As can be seen, all the reconstructions are very accurate, thus confirming the effectiveness of the approach.

It is interesting to compare the number of data (2 721) needed by the described NF–FF transformation with spherical spiral scanning with that (3 280) required by MI software package implementing the classical NF–FF transformation with spherical scanning [10]. In particular, the number of "regular samples" at spacing $\Delta\eta$ is 2 433, whereas the number of "extra samples" at reduced spacing is 288.

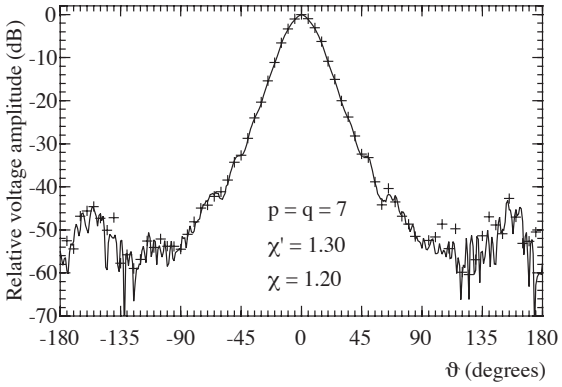

Figure 3 - Amplitude of V_1 on the meridian at φ = 0°. Solid line: measured. Crosses: recovered from NF data acquired via the spherical spiral scanning.

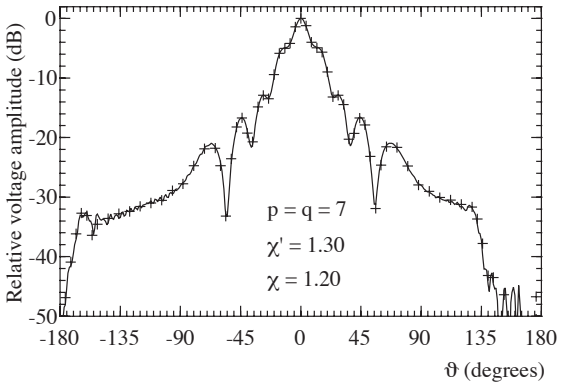

Figure 4 - Amplitude of V_2 on the meridian at φ = 90°. Solid line: measured. Crosses: recovered from NF data acquired via the spherical spiral scanning.

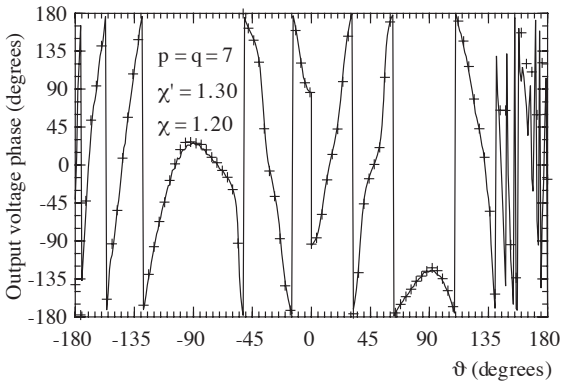

Figure 5 - Phase of V_2 on the meridian at φ = 90°. Solid line: measured. Crosses: recovered from NF data acquired via the spherical spiral scanning.

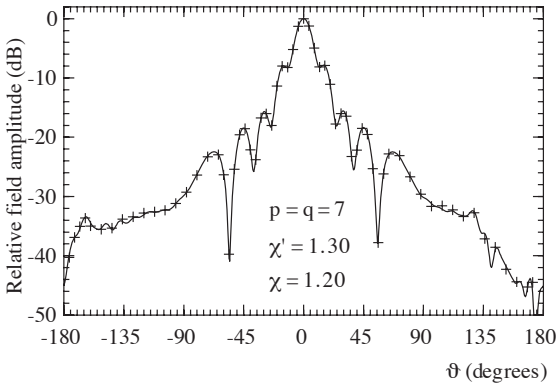

Figure 6 – E-plane pattern. Solid line: reference. Crosses: recovered from NF data acquired via the spherical spiral scanning.

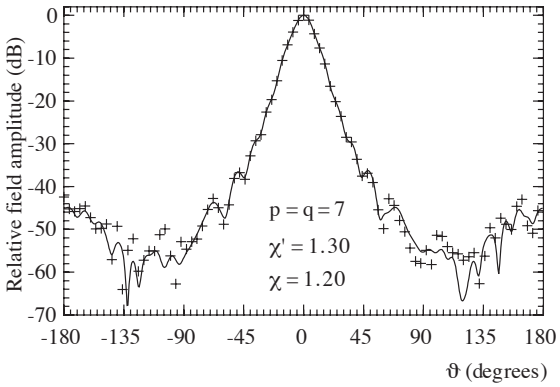

Figure 7 - H-plane pattern. Solid line: reference. Crosses: recovered from NF data acquired via the spherical spiral scanning.

4. Conclusion and future developments

An experimental validation of the NF–FF transformation with spherical spiral scanning using a spherical modelling of the AUT has been provided in this work. A very good agreement has been found both in the near-field and in the far-field reconstructions, thus demonstrating that such an innovative transformation, which allows a drastic reduction of the measurement time, retains the accuracy of the classical spherical one. On the basis of theoretical results, it has to be expected that the measurement time as well as the number of required NF data can be further reduced by using spherical spiral scanning techniques based on more effective antenna modellings, which fit better the actual antenna geometry. Future developments will just regard the experimental validation of the NF–FF transformations with spherical spiral scanning for elongated and quasi-planar antennas using the aforementioned effective modellings.

5. REFERENCES

[1] J. Appel-Hansen, J.D. Dyson, E.S. Gillespie, and T.G. Hickman, "Antenna measurements," in *The Handbook of Antenna Design*, A. W. Rudge, K. Milne, A.D. Olver, and P. Knight (Eds.), Peter Peregrinus Ltd., London, UK, 1982.

[2] A.D. Yaghjian, "An overview of near-field antenna measurements," *IEEE Trans. Antennas Propagat.,* vol. AP-34, pp. 30-45, 1986.

[3] E.S. Gillespie (Ed.), "Special Issue on near-field scanning techniques," *IEEE Trans. Antennas Propagat.,* vol. AP-36, pp. 727-901, 1988.

[4] C. Gennarelli, G. Riccio, F. D'Agostino, and F. Ferrara, *Near-field – far-field transformation techniques*, vol. 1, CUES, Salerno, Italy, 2004.

[5] M.H. Francis and R.W. Wittmann, "Near-field scanning measurements: theory and practice," chapter 19 in *Modern Antenna Handbook*, C.A. Balanis, (Ed.), John Wiley & Sons, Inc., Hoboken, NJ, USA, 2008.

[6] C. Gennarelli, A. Capozzoli, L. Foged, J. Fordham, and D.J. van Rensburg (Eds.), "Special Issue on Recent advances in near-field to far-field transformation techniques," *Int. Jour. Antennas Propagat.*, vol. 2012.

[7] P.F. Wacker, "Non-planar near-field measurements: Spherical scanning," NBSIR 75-809, Boulder, CO, 1975.

[8] F.H. Larsen, "Probe correction of spherical near-field measurements," *Electronic Letters*, vol. 13, No. 14, 1977, pp. 393–395.

[9] A.D. Yaghjian and R.C. Wittmann, "The receiving antenna as a linear differential operator: application to spherical near-field measurements," *IEEE Trans. Antennas Propagat.,* vol. AP-33, pp. 1175-1185, 1985.

[10] J. Hald, J.E. Hansen, F. Jensen, and F.H. Larsen, *Spherical Near-Field Antenna Measurements*, J.E. Hansen (Ed.), Peter Peregrinus Ltd., London, UK, 1988.

[11] O.M. Bucci, F. D'Agostino, C. Gennarelli, G. Riccio, and C. Savarese, "Data reduction in the NF–FF transformation technique with spherical scanning," *Jour. Electromagn. Waves Appl.,* vol. 15, pp. 755-775, 2001.

[12] A. Arena, F. D'Agostino, C. Gennarelli, and G. Riccio, "Probe compensated NF–FF transformation with spherical scanning from a minimum number of data," *Atti della Fondazione G. Ronchi,* vol. 59, pp. 312-326, 2004.

[13] F. D'Agostino, F. Ferrara, C. Gennarelli, R. Guerriero, and M. Migliozzi, "Effective antenna modellings for a NF–FF transformation with spherical scanning using the minimum number of data," *Int. Jour. Antennas Propagat.*, vol. 2011, ID 936781, 11 pages.

[14] T.B. Hansen, "Higher-order probes in spherical near-field scanning," *IEEE Trans. Antennas Propagat.,* vol. 59, pp. 4049-4059, 2011.

[15] R.G. Yaccarino, L.I. Williams, and Y. Rahmat-Samii, "Linear spiral sampling for the bipolar planar antenna measurement technique," *IEEE Trans. Antennas Propagat.,* vol. AP-44, pp. 1049-1051, 1996.

[16] O.M. Bucci, F. D'Agostino, C. Gennarelli, G. Riccio,

and C. Savarese, "NF–FF transformation with spherical spiral scanning," *IEEE Antennas Wireless Propagat. Lett.*, vol. 2, pp. 263-266, 2003.

[17] F. D'Agostino, C. Gennarelli, G. Riccio, and C. Savarese, "Theoretical foundations of near-field–far-field transformations with spiral scannings," *Prog. in Electromagn. Res.,* vol. PIER 61, pp. 193-214, 2006.

[18] F. D'Agostino, F. Ferrara, C. Gennarelli, R. Guerriero, M. Migliozzi, and G. Riccio, "A nonredundant near-field to far-field transformation with spherical spiral scanning for nonspherical antennas," *The Open Electrical & Electronic Eng. Jour.,* vol. 3, pp. 4-11, 2009.

[19] F. D'Agostino, F. Ferrara, C. Gennarelli, R. Guerriero, and M. Migliozzi, "Far–field reconstruction from a minimum number of spherical spiral data using effective antenna modellings", *Prog. in Electromagn. Res. B,* vol. 37, pp. 43-58, 2012.

[20] O.M. Bucci, C. Gennarelli, and C. Savarese, "Representation of electromagnetic fields over arbitrary surfaces by a finite and nonredundant number of samples," *IEEE Trans. Antennas Propagat.*, vol. 46, pp. 351-359, 1998.

[21] O.M. Bucci, C. Gennarelli, and C. Savarese, "Optimal interpolation of radiated fields over a sphere," *IEEE Trans. Antennas Propagat.,* vol. AP-39, pp. 1633-1643, 1991.

[22] F. D'Agostino, F. Ferrara, C. Gennarelli, R. Guerriero, and M. Migliozzi, "The unified theory of near–field – far–field transformations with spiral scannings for nonspherical antennas," *Prog. in Electromagn. Res. B,* vol. 14, pp. 449-477, 2009.

[23] O.M. Bucci, G. D'Elia, and M.D. Migliore, "Advanced field interpolation from plane-polar samples: experimental verification," *IEEE Trans. Antennas Propagat.,* vol. 46, pp. 204-210, 1998.